Imaging performance evaluation in depth-of-interaction PET with a new method of sinogram generation: A Monte Carlo simulation study

XIA Yan[1,2] MA Tianyu[1] LIU Yaqiang[1,*] SUN Xishan[2] WANG Shi[1] SHAO Yiping[2]

[1]*Department of Engineering Physics, Key Laboratory of Particle & Radiation Imaging (Tsinghua University), Ministry of Education, Beijing 100084, China*

[2]*Department of Imaging Physics, University of Texas M.D. Anderson Cancer Center, Houston, Texas 77030, USA*

Abstract In conventional PET systems, the parallax error degrades image resolution and causes image distortion. To remedy this, a PET ring diameter has to be much larger than the required size of field of view (FOV), and therefore the cost goes up. Measurement of depth-of-interaction (DOI) information is effective to reduce the parallax error and improve the image quality. This study is aimed at developing a practical method to incorporate DOI information in PET sinogram generation and image reconstruction processes and evaluate its efficacy through Monte Carlo simulation. An animal PET system with 30-mm long LSO crystals and 2-mm DOI measurement accuracy was simulated and list-mode PET data were collected. A sinogram generation method was proposed to bin each coincidence event to the correct LOR location according to both incident crystal indices and DOI positions of the two annihilation photons. The sinograms were reconstructed with an iterative OSMAPEM (ordered subset maximum *a posteriori* expectation maximization) algorithm. Two phantoms (a rod source phantom and a Derenzo phantom) were simulated, and the benefits of DOI were investigated in terms of reconstructed source diameter (FWHM) and source positioning accuracy. The results demonstrate that the proposed method works well to incorporate DOI information in data processing, which not only overcomes the image distortion problem but also significantly improves image resolution and resolution uniformity and results in satisfactory image quality.

Key words Positron emission tomography (PET), Depth of interaction (DOI), Monte Carlo simulation, Sinogram generation, Image reconstruction

1 Introduction

Positron Emission Tomography (PET) has been widely used in clinical and pre-clinical applications. Among many modalities of radiological *in vivo* imaging, PET is promising for providing functional, metabolic and molecular information of human and animals.

In practice, improving PET resolution and sensitivity, and expanding PET applications at low cost, stands for the most focused development requirements. A major challenge in realizing a low cost and high performance PET system is parallax error. As shown in Fig.1, when the annihilation locates off the center of field of view (FOV), the related line of response (LOR) is not along the long-axis of the incident crystals, and LOR positioning error occurs, which will further distort reconstruction of sources. This effect is referred to as parallax error effect. In general, the longer the crystal is, the severer the parallax error effect becomes. However, the need of high sensitivity leads to employment of longer crystals. For example, the detection efficiency of 511 keV photons in LSO crystal (lutetium oxy-orthosilicate) increases from 34.1% to 86.1% when the crystal length changes from 10 mm to 30 mm.

One way to get an acceptable tradeoff between relief of parallax error and sensitivity is to build larger

Supported by Specialized Research Fund of the Doctoral Program of Higher Education (SRFDP 200800031071), National Natural Science Foundation of China (No.10975086) and National High Technology Research and Development Program (“863” Program) of China (No.2006AA020802)

* Corresponding author. *E-mail address:* liuyaqiang@mail.tsinghua.edu.cn

Received date: 2011-02-22

detector ring but choose relatively small FOV, typically 50%–60% of the detector diameter[1]. In this way, the regions that are highly affected by parallax error are omitted from FOV, but overall system cost increases accordingly. Another way to reduce the parallax error impact, without cost increase and obvious sensitivity loss, is to measure the depth-of-interaction (DOI) information. In PET detectors, DOI incorporation brings the following benefits[1-4]: (a) better spatial resolution and spatial resolution uniformity; (b) improved recovery of source intensity distribution; (c) more accurate radiation source positioning; and (d) lower cost by achieving the same FOV size with reduced ring diameter. In recent years, DOI detector and system development has attracted considerable interest of researchers.

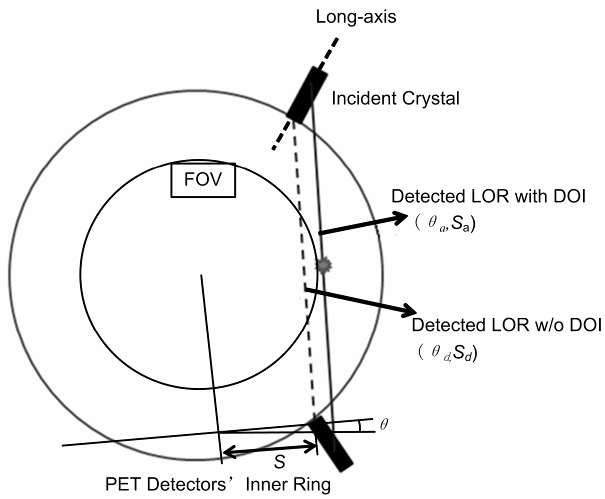

Fig.1 Parallax error caused by the lack of DOI detection.

There are mainly three approaches to obtain the DOI information:

(a) Pulse height detection (PHD) method [5-7], in which the output pulse signals are read from either one end or both ends of the crystal, and the DOI is estimated as a function of the pulse heights or the ratio of the observed output signals[8-12].

(b) Pulse shape detection (PSD) method[13-15], in which the detectors are of multiple layers and crystals using phoswich technology, and pulse shape discrimination technique is introduced to distinguish different pulse decay constants and differentiate the events captured in different layers.

(c) Light sharing method [16,17], which uses multi-layered detectors, too, but the layers are of the same type of crystal. The key technology is to finely design the reflective films in between the crystals to control optical photon spread path inside and between the layers. The design should assure that gamma photons deposited in different crystals or different layers will generate different light spread and PMT readout.

With current techniques, 2-mm resolution (FWHM), the best DOI resolution reported so far [9,10], is chosen to validate the present method. A Monte Carlo simulation package is used to set up an animal PET system with 30-mm LSO crystals and execute the acquisition process. A new sinogram generation method is proposed to incorporate DOI information into the sinogram generation process. Imaging performance is studied through reconstructed images of different simulated phantoms. The PET systems and methods used in data simulation, sinogram generation and image reconstruction are described in Section 2. The reconstructed images of a rod-source phantom and a Derenzo phantom with and without DOI are compared and discussed in Section 3.

2 Materials and Methods

2.1 Simulated PET system, sources and acquisition process

A cylindrical animal PET system (Fig.2) is simulated in this study. Each of the four detector rings has 24 detector blocks, and each block has 12×12 LSO crystals of 1.59 mm×1.59 mm×30 mm. The PET system has an inner ring of 73.6-mm radius and 50-mm FOV.

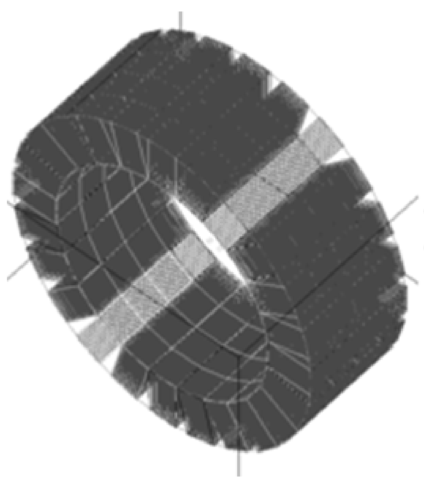

Fig.2 Configuration of a PET simulated in GATE.

The system is modeled in a Monte Carlo simulation package GATE (GEANT4 application for tomographic emission)[18]. GATE has been widely used in simulation of nuclear medicine imaging systems, because it can simulate the emission, transportation and detection of positron and gamma photon sources, mimic the data acquisition process of PET systems and produce list-mode coincidence events data in ROOT-format file[19]. It has been demonstrated that GATE can produce simulation results with reasonable accuracy compared to experimental measurements[20].

Two routine phantoms were simulated. The first one is a line of rod-source phantom (see Fig.3a for its transaxial view). It has 7 hot-rod sources (Φ1.5 mm×2 mm, 0.08 mCi each) aligned from the center to the right-most edge of FOV and denoted as 1 to 7 only for later comparison convenience. The second one is a Derenzo phantom, with its transaxial view shown in Fig.3b. The radius and length of the phantom are 45 mm and 3.18 mm, respectively. The phantom is divided into 6 rod sections in diameter of 1.2, 1.6, 2.4, 3.2, 4.0 and 4.8 mm respectively. The rods in each section are arranged in an equilateral triangle shape. The separation between adjacent rods equals twice the corresponding rod diameter. A line of rods crossing 3.2 mm section and 4.8 mm have denotations, too, for later comparison.

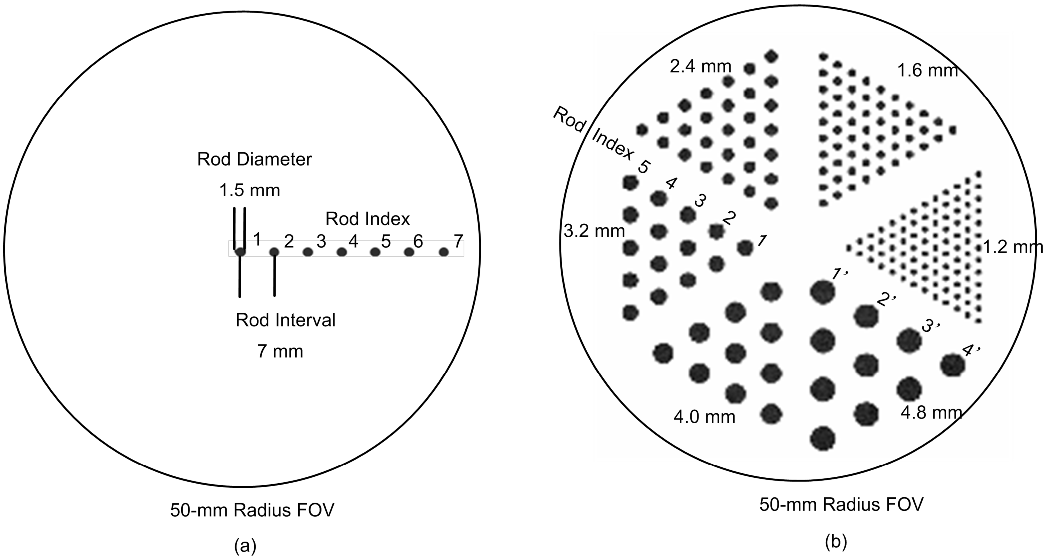

Fig.3 Rod-source phantom (a) and Derenzo phantom (b) in transverse view.

The PET system was simulated in 2D mode, the maximum ring difference was set to 6, and the acquisition time was set to 10 seconds. The simulations were run on a workstation with Intel Xeon 5520 CPU and 4 GB RAM. It took 30 CPU hours to complete simulation for the rod-source phantom and 5.6 hours for the Derenzo phantom, with a total of 3.7 M and 1.9 M accumulated coincidence events, respectively.

2.2 Sinogram generation incorporating DOI information

The routine implementation of histogramming is to build a one-to-one mapping between possible LORs and sinogram bins. For example, when a coincidence event is captured in crystal m and n, and the DOI information is unknown, (m, n) is a necessary and sufficient indicator of the LOR related to the two crystals. Correspondingly, a quasi sinogram is defined, within which each sampling bin corresponds to one pair of crystal indices, too. An arc-correction procedure is needed to convert the non-uniformly defined quasi sinogram to a uniformly sampled one to make it a proper input format of reconstruction procedure.

The DOI incorporation increases significantly the amount of LOR. In order to keep original sinogram size and skip the arc correction, we found a different histogramming approach: First, a uniform sinogram, instead of a traditional quasi sonogram, is defined, and each bin (θ_i, S_j) stands for a range of sampling angle θ and sampling offset S, as defined in Fig.1. Cartesian coordinates of each event, rather than the crystal indices, are used to calculate LOR actual sample information of (θ_a, S_a). We note that (θ_a, S_a) is not one-to-one mapping to the bins of sinogram, so this event is binned into 4 bins nearest to (θ_a, S_a), as shown in Fig.4, with weights calculated by a 2D linear interpolation, reversely proportional to the distance from (θ_a, S_a) to (θ_i, S_j). A similar approach in Ref.[21] addresses the upsampling problem, though the work aimed at developing multi-layer detectors with a rounding logic in the histogramming process, which is different from the interpolation method used in this study.

In the present study, based on PET spatial resolution limit, 144 angular and 129 radial sinogram bins were chosen to cover all the LORs. No correction and normalization were applied in current stage.

The non-DOI and 2-mm DOI measurements are shown in Fig.5. Fig.5a shows that the most current non-DOI PET, the detected position is assigned to the crystal surface center, while in Fig.5b, the 2-mm DOI, the measured depth is supposed to follow a Gaussian distribution, with an FWHM of 2 mm. Namely, when a true DOI of an incident gamma photon is generated by GATE, the detector response blurs the true position defined by the Gaussian distribution, and randomly generates a blurred depth as the detection result.

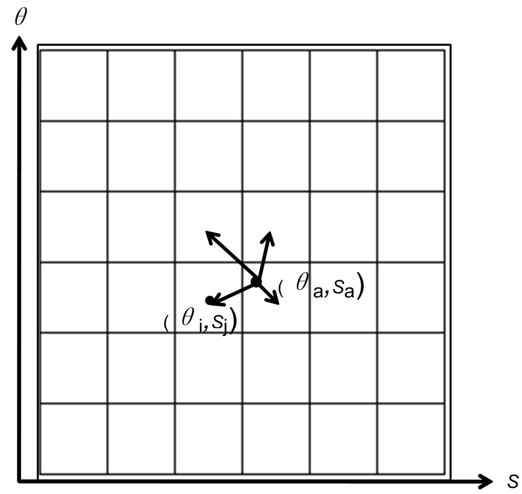

Fig.4 Sinogram generation interpolation.

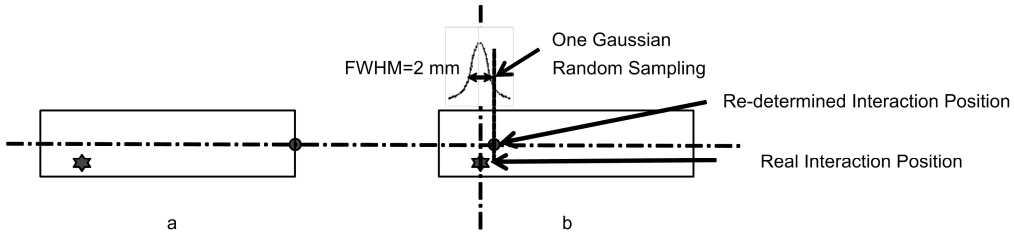

Fig.5 Schematics of the non-DOI (a) and 2-mm DOI (b) measurements.

2.3 Image reconstruction

A PET image reconstruction package, STIR (Software for Tomographic Image Reconstruction)[22] was used. The sinogram was formatted to be compatible with STIR program. Ordered-subset maximum-a-posteriori expectation-maximization(OSMAPEM) algorithm was used to reconstruct the sinogram data with 10 iterations and 4 ordered subsets. A filtered root mean prior was applied and the penalization factor was set at β=0.2.

3 Results and discussion

3.1 Rod source phantom studies

Reconstructed images of the lined rod-source phantom incorporating none DOI information are shown in Fig.6a. The image accords to our knowledge of non-DOI PET that it suffers from parallax error, and shows severer radial elongation towards the FOV edge. The image using sinogram generated by the method incorporating 2-mm DOI resolution is shown in Fig.6b, where the elongation effect is almost eliminated, and obvious improvements of the resolution and resolution uniformity can be observed throughout the FOV. More details can be found in Fig.6c, which shows the horizontal line profiles of Figs.6a and 6b.

To do a quantitative study on impact of incorporating DOI information and to validate the proposed sinogram generation method, two figures of merit (FOM), i.e. the rod position and reconstructed rod diameter, were chosen to evaluate the imaging quality. The first FOM aims at validating LOR positioning precision, and the second one could be an indicator of resolution and resolution uniformity. The calculation process of the two FOMs is as follows: to each rod profile, a standard Gaussian function is fitted by the least square rule, and the mean radial distance of fitted Gaussian curve is treated as reconstructed rod diameter and the FWHM as the rod position.

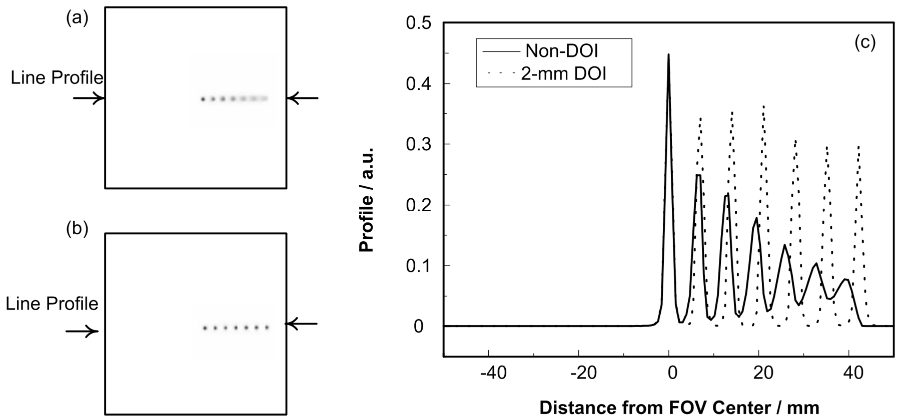

Fig.6 Reconstructed images of the rod-source phantom: (a) non-DOI, (b) 2-mm FWHM DOI, (c) profiles of horizontal central lines crossing the rods.

Plot of the two FOMs as function of rod radial distance is shown in Fig.7. Fig.7a shows the rod positions of non-DOI case (■) and the 2-mm DOI case (◆), and true rod position (—) as reference. Mean positioning error of the non-DOI case is −3.16 mm, while it improves to 0.29 mm for the 2-mm DOI case. This confirms that parallax error will cause off-center source positioning in the reconstructed image, always shifting from its true position towards FOV center in cylindrical PET. Fig.7b is the reconstructed rod diameter (FWHM) of the non-DOI case (■), and 2-mm DOI case (◆). One sees that resolution of the non-DOI system gets worse rapidly when source goes towards the FOV edge, but it changes slightly for the 2-mm DOI system, with the standard deviation of the seven rods being just 0.14-mm, in contrast to the 0.80-mm SD of the non-DOI FWHM system.

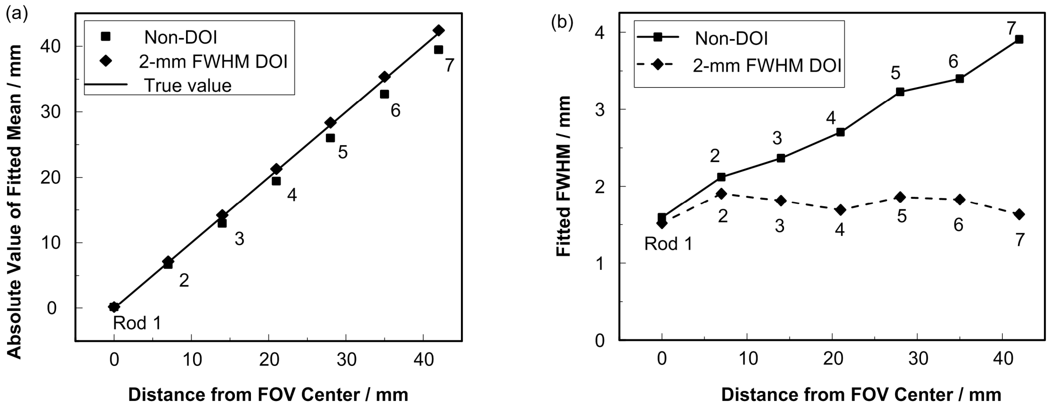

Fig.7 Reconstructed rod position (Gaussian mean) and diameter (Gaussian FWHM) as functions of distance from FOV center for the lined rod-source. The numbers are denoted for the rod sources in Fig.3a.

3.2 Derenzo phantom studies

The same simulation, post process and analysis were executed with the Derenzo phantom. Results of images and figures are similarly structured as those of lined rod-source phantom in Section 3.1.

Reconstructed images of the non-DOI and 2 mm DOI systems are shown as Figs.8a and 8b, respectively, and profiles crossing 3.2 mm and 4.8 mm sections are plotted in Fig.8c. In Fig.8a, section of 3.2 mm is a little blurred, while in Fig.8b the rods can be well distinguished. Imaging standard Derenzo phantom is an acknowledged tool used widely in practice to determine overall resolution performance of a system. In this sense, at least 0.8-mm resolution improvement is confirmed when involving 2-mm DOI information in the simulated system. Also, a 'shrink' effect of the non-DOI system can be seen by comparing Figs.8a and 8b. This is caused by the source positioning error towards FOV center.

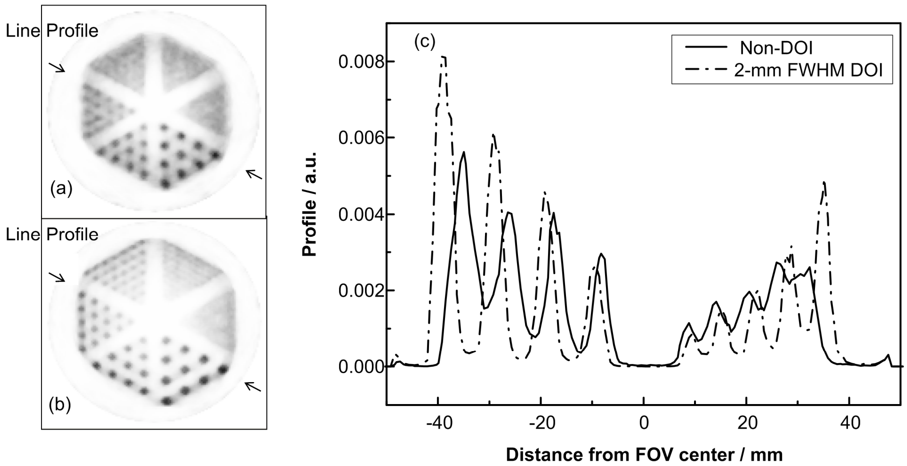

Fig.8 Reconstruction images of Derenzo phantom: (a) non-DOI, (b) 2-mm FWHM DOI, (c) profiles of central lines crossing the rods.

Figure 9 shows the FOM of the rod position and reconstructed rod diameter. From Fig.9a, the mean positioning errors for non-DOI and 2-mm DOI systems are −1.53 mm and 0.46 mm, respectively. In Fig.9b, resolution of the non-DOI system deteriorates when the source location goes off the FOV center, with the standard deviation of FWHM being 1.09 and 0.59 mm in sections of 3.2 and 4.8 mm, respectively, while the FWHMs of 2-mm DOI-PET system differ little from each other, with 0.20-mm and 0.12-mm SD in 3.2 and 4.8 mm sections, respectively.

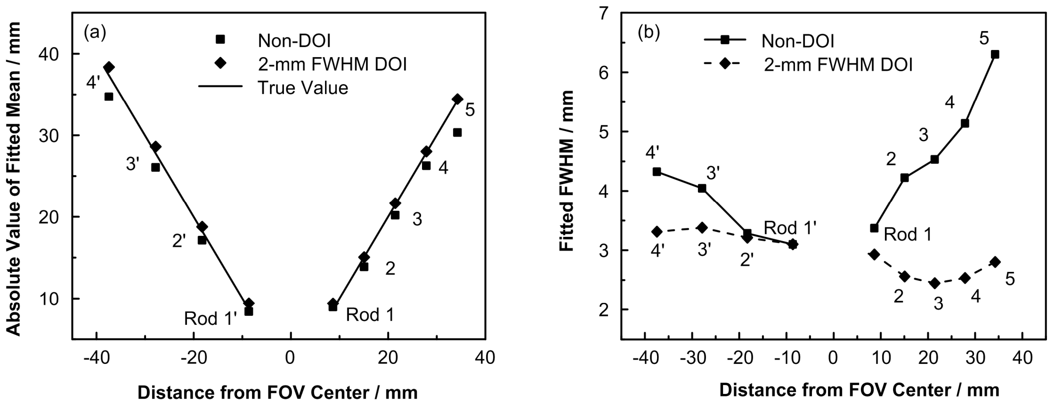

Fig.9 Reconstructed rod position (Gaussian mean) (a) and diameter (Gaussian FWHM) (b) as functions of distance from FOV center in Derenzo study. The numbers are denoted for the rod sources in Fig.3b.

Benefits of DOI information mentioned in Section 1 are confirmed by the lined rod-source phantom and Derenzo phantom. The sinogram generation method skipped the definition of quasi sinogram and arc correction to generate sinogram directly, and simulation results demonstrate that the proposed method can well incorporate DOI information and yield images of better positioning, higher spatial resolution and improved spatial resolution uniformity across the entire FOV.

4 Conclusion

DOI was at first brought forward to solve parallax error and the mechanical detection method has been on research widely in recent years, but the post processing method on how to incorporate DOI method was less reported. In this work, we propose a practical method to incorporate DOI information into the PET sinogram generation process. Uniform distributed sinogram is directly defined, and LOR of a coincident event, denoted as (θ_a, S_a), is calculate based on detected coordinates of gamma pairs directly. Then an interpolation process is employed to bin this event into 4 neighborhood bins of the uniform sinogram.

By our sinogram generation method, the benefit of DOI-PET system development was investigated through Monte Carlo simulations. Reconstructed images demonstrate the importance of measuring DOI information for a dedicated compact-size PET for small animal imaging. With 2mm DOI measurement accuracy, the minimum rod diameter that can be distinguished in Derenzo phantom improves from 3.2 mm to 2.4 mm, and much better image resolution uniformity and source positioning can be achieved as well. All these will significantly improve the overall image quality.

It can be concluded that satisfactory image quality is achievable for a PET with 30 mm crystal, 2-mm DOI measurement accuracy and proposed DOI information incorporation method. It will significantly improve the system sensitivity without substantial overall system cost increasing. In future work, we will seek for advanced sinogram processing and image reconstruction methods to take full advantages of DOI information for further improving the performance of a DOI-PET.

References

1 Chen C T, Pan X C, Kao C M. United States Patent: US 006528791B1. Mar. 4, 2003.

2 Levin C S, Zaidi H. PET Clin, 2007, **2:** 125–160.

3 Kao C M, Pan X C, Chen C T. IEEE Trans Nucl Sci, 2000, **47:** 1551−1560.

4 Shao Y P, Meadors K, Silverman R W, *et al*. IEEE Trans Nucl Sci, 2002, **49:** 649–654.

5 Moses W W, Derenzo S E. IEEE Trans Nucl Sci, 1994, **41:** 1441–1445.

6 Moisan C, Andreaco M S, Rogers J G, *et al*. IEEE Trans Nucl Sci, 1998, **45:** 3030–3035.

7 Miyaoka R S, Lewellen T K, Yu H, *et al*. IEEE Trans Nucl Sci, 1998, **45:** 1069–1073.

8 Shao Y P, Li H R, Gao K K. Nucl Instrum Methods Phys Res A, **580:** 944–950.

9 Yang Y F, Qi J Y, Wu Y B, *et al*. Phys Med Biol, 2009, **54:** 433–435.

10 Shao Y P, Yao R T, Ma T Y. Med Phys, 2008, **35:** 5829-5840.

11 Dokhale P A, Silverman R W, Shah K S, *et al*. Phys Med Biol, 2004, **49:** 4293–4304.

12 Burr K C, Ivan A, Castleberry D E, *et al*. IEEE Trans Nucl Sci, 2004, **51:** 1791–1798.

13 Saoudi A, Pepin C M, Dion F, *et al*. IEEE Trans Nucl Sci, 1999, **46:** 462–467.

14 Eriksson L, Wienhard K, Eriksson M, *et al*. IEEE Trans Nucl Sci, 2002, **49:** 2085–2088.

15 Du H N, Yang Y F, Glodo J, *et al*. Phys Med Biol, 2009, **54:** 1757–1771.

16 Tsuda T, Murayama H, Kitamura K, *et al*. IEEE Trans Nucl Sci, 2004, **51:** 2537–2542.

17 Inadama N, Murayama H, Hamamoto M. *et al*. IEEE Trans Nucl Sci, 2006, **53:** 2523–2528.

18 Jan S, Santin G, Strul D, *et al*. Phys Med Biol, 2004, **49:** 4543–4561.

19 ROOT. An Object-Oriented Data Analysis Framework. http://root.cern.ch/drupal/.

20 Lazaro D, Buvat I, Strul D, *et al*. Phys Med Biol, 2004, **49:** 271–285.

21 Perera L, Lerch M, Rosenfeld A B, *et al*. IEEE Nuclear Science Symp Conf Record, 2007, 3754–3759.

22 STIR. Software for Tomographic Imaging Reconstruction. http://stir.sourceforge.net.